LANGMUIR

pubs.acs.org/Langmuir Article

Transparent Films Made of Highly Scattering Particles

Talha Erdem,* Lan Yang, Peicheng Xu, Yemliha Altintas, Thomas O'Neil, Alessio Caciagli, Caterina Ducati, Evren Mutlugun, Oren A. Scherman, and Erika Eiser*

Cite This: *Langmuir* 2020, 36, 911−918 Read Online

ACCESS | Metrics & More | Article Recommendations | Supporting Information

ABSTRACT: Today, colloids are widely employed in various products from creams and coatings to electronics. The ability to control their chemical, optical, or electronic features by controlling their size and shape explains why these materials are so widely preferred. Nevertheless, altering some of these properties may also lead to some undesired side effects, one of which is an increase in optical scattering upon concentration. Here, we address this strong scattering issue in films made of binary colloidal suspensions. In particular, we focus on raspberry-type polymeric particles made of a spherical polystyrene core decorated by small hemispherical domains of acrylate with an overall positive charge, which display an unusual stability against aggregation in aqueous solutions. Their solid films display a brilliant red color due to Bragg scattering but appear completely white on account of strong scattering otherwise. To suppress the scattering and induce transparency, we prepared films by hybridizing them with oppositely charged PS particles with a size similar to that of the bumps on the raspberries. We report that the smaller PS particles prevent raspberry particle aggregation in solid films and suppress scattering by decreasing the spatial variation of the refractive index inside the film. We believe that the results presented here provide a simple strategy to suppress strong scattering of larger particles to be used in optical coatings.

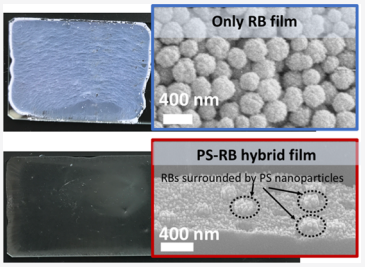

INTRODUCTION

Colloidal nanoparticles are commonly employed in various applications,[1] including optical coatings,[2] optoelectronic devices,[3,4] sensing,[5−8] photovoltaics,[9−11] electronics,[12−14] and bioimaging,[15−19] to name a few. Today, they possess an invaluable place in various branches of science and engineering as they enable control over reactivity, stability, size, and shape, all of which allow for tuning their physical, electronic, chemical, and optical features.

An important advantage that colloidal nanoparticles offer is the increased surface area per volume, that is, the surface-to-volume ratio. Increasing this ratio enables improved stability in dispersions,[20] enhances interaction with surrounding materials,[21] and helps transfer charges[22] that may be especially of interest for sensing and photovoltaics. One of the strategies to increase the surface-to-volume ratio is decreasing the size of the nanoparticles as this ratio is proportional to the inverse of the radius for a spherical particle (surface/volume $\propto r^2/r^3 \propto 1/r$). Nevertheless, this approach may be sometimes unpractical or undesirable. Another strategy that is commonly exploited to increase this ratio is utilizing nanoparticles with rough surfaces.[23] Placing bumps with a well-defined size on the surfaces of smooth particles boosts the surface-to-volume ratio, which offers advantages without substantially changing the size of the colloids. For example, we previously showed that aqueous suspensions of raspberry particles (called RBs hereafter) that are made of a spherical polystyrene core particle densely coated with smaller polyacrylate nanoparticles exhibit unexpected stability even at very high added salt concentrations.[24] This stability was provided by the high surface charge of these particles along with their specific surface-to-volume ratio.

An important optical feature of these RB particles is their increasing optical scattering, which may not be a desired feature for some applications. To address this problem, we present here a simple methodology to suppress the optical scattering of the solid films by hybridizing these RB particles with either polymeric nanoparticles or quantum dots. Our strategy relies on placing the RBs together with smaller, oppositely charged transparent nanoparticles. We show that, when these nanoparticles are bound to our RB particles via Coulomb attractions, the resulting composite RB particles do not aggregate and form solid films different from films made of only RB particles, leading to increased transparency. We effectively demonstrate that placing the large scattering particles in a sea of small ones reduces the refractive index variation, leading to decreased scattering despite the roughness of the films. We believe that the simple methodology we propose here may make various types of organic and inorganic nanoparticles suitable for photonic and electronic applications by suppressing their scattering.

Received: April 5, 2019
Revised: January 13, 2020
Published: January 13, 2020

https://dx.doi.org/10.1021/acs.langmuir.9b01014
Langmuir 2020, 36, 911−918

EXPERIMENTAL METHODS

Synthesis of Raspberry Particles. Following the synthesis introduced by Lan et al.,[24] 2.08 g of styrene (St; 2.08 g, 20.0 mmol), 130 mg of divinylbenzene (DVB), and 428 mg of 2-(methacryloyloxy)ethyl acetoacetate (AM) were loaded into a 50 mL water/ethanol mixture with a ratio of 80/20% v/v. Subsequently, 54 mg of 2,2′-azobis(2-methylpropionamide) dihydrochloride (AIBA) was added to the mixture, kept under a N_2 atmosphere for 1 h, and then heated to 70 °C. The reaction continued for 24 h. Synthesized raspberry particles were then purified by dialysis against water for 5 days.

Synthesis of Negatively Charged Polystyrene Nanoparticles. Sodium 4-vinylbenzenesulfonate (SVBS; 660 mg) and potassium persulfate (KPS; 135 mg) were dissolved in 100 mL of deionized water. The mixture was then sealed and degassed by cycling vacuum and nitrogen five times before being heated to 70 °C with vigorous stirring. Styrene (5.2 g) was injected immediately. After 24 h, the reaction was stopped by quenching the reaction vessel on ice and the nanoparticles were washed by dialysis.

Synthesis of Positively Charged Polystyrene Nanoparticles. Methyl iodide (5 mL) dissolved in dichloromethane (DCM; 50 mL) was added dropwise to a solution of bipyridine (10 g) in 100 mL of DCM with vigorous stirring and left to react for 24 h. 1,1′-Dimethyl-[4,4′-bipyridine]-1,1′-diium iodide (MV+) was collected by filtration and drying. A solution of MV+ (6.02 g) in acetonitrile (300 mL) was prepared at 80 °C and allowed to cool to 60 °C. 4-Vinylbenzyl chloride (10 mL) was added and the reaction allowed to proceed for 24 h. 1-Methyl-1′-(4-vinylbenzyl)-[4,4′-bipyridine]-1,1′-diium chloride iodide (StMV) was collected by filtration and drying.

StMV (7 mg for 280 nm particles, 90 mg for 45 nm particles) and 2,2′-azobis(2-methylpropionamidine) dihydrochloride (AIBA) (25 mg) were dissolved in 100 mL of water and the solution degassed by cycling vacuum and nitrogen five times. The solution was heated to 80 °C with vigorous stirring, and styrene (5.2 g) was injected immediately. After 24 h, the reaction was stopped by quenching the reaction vessel on ice, and the nanoparticles were washed by dialysis.

Synthesis of InP/ZnS Core/Shell Nanocrystal Quantum Dots. InP/ZnS quantum dots were synthesized using a recipe developed by Altintas et al.[25] with some modifications of the synthesis procedure. Briefly, 0.12 mmol of indium acetate, 0.36 mmol of myristic acid, and 6 mL of 1-octadecene (ODE) were mixed in a three-necked 25 mL flask, degassed for 5 min, and then purged with Ar gas for 5 min. This procedure was repeated three times to remove dissolved oxygen and other impurities. Subsequently, the solution was heated to 100 °C under vacuum (3×10^{-3} mbar) and kept at this pressure for 1.5 h to obtain a clear solution. This clear solution was then cooled down to room temperature. A successive vacuum-gas procedure was used, and the temperature was increased to 220 °C after addition of 1 mmol of Zn stearate purum and 0.025 mmol of 1-dodecanethiol (DDT). Tris(trimethylsilyl)phosphine ($(TMS)_3P$) as a phosphor source (0.08 mmol of $(TMS)_3P$ in 1 mL of ODE prepared in the glovebox) was quickly injected into the flask after reheating to 220 °C. Next, the InP core quantum dots were grown at 285 °C for 10 min. After cooling down the flask to room temperature, the shell was coated by adding 0.2 mmol of Zn stearate (purum) at room temperature and then applying a successive vacuum-gas conversion procedure. The temperature of the flask was increased to 230 °C under a Ar atmosphere and kept for 3 h. DDT (0.4 mmol) was added dropwise (prepared in 1 mL of ODE) into the flask and kept further for 1 h. After cooling back to room temperature, the crude solution of the synthesis was transferred into a 50 mL centrifuge tube by adding 5 mL of hexane and centrifuged two times at 5000 rpm for 8 min to separate unreacted species via discarding the precipitated particles. Acetone (25 mL) and methanol (3 mL) were added into the supernatant solution and then precipitated by centrifugation at 5000 rpm for 10 min and dissolved in hexane. The precipitation method was carried out two times with the method described, and finally, the synthesized QDs were redispersed in hexane.

Phase Transfer of the Quantum Dots. The QDs dispersed in chloroform were transferred to the water phase using a methodology described in ref 26. The procedure involved coating the QDs with an amphiphilic polymer. This polymer was synthesized by first dissolving 3.084 g of poly(isobutylene-*alt*-maleic anhydride) and 3.5 mL of dodecylamine in 100 mL of tetrahydrofuran (THF) in a round flask. The mixture was vigorously stirred and then kept at 60 °C for 3 h; subsequently, the reaction mixture was concentrated to approximately five times of its original QD content using a rotary evaporator and kept at 60 °C overnight. Then, the mixture was completely dried using again a rotary evaporator and dissolved in 25 mL of chloroform such that the final concentration of the monomer units becomes 0.8 M. Next, 250 μL of the QDs (~20 μM) was mixed with 0.8 mL of the synthesized polymer, and the mixture was slowly evaporated using a rotary evaporator. The resulting solid was then dissolved in 0.1 M NaOH and sonicated. To remove large aggregates, the mixture was filtered using a 0.22 μm syringe filter. Finally, the QDs were redispersed into a TAE buffer by using an ultracentrifuge filter unit (100 kDa).

Molar Concentration Estimates of the Nanoparticles. The molar concentration of the RBs was estimated by calculating their molecular weight and measuring the density of the dispersion. For this purpose, we first calculated the number of polyacrylate half spheres of 45 nm in diameter that can fit on the surface of 235 nm sized PS nanoparticles. The number was obtained by a Monte Carlo simulation of hard disks near random close packing using spherical boundary conditions, according to the scheme described in ref 27. The radius of the PS nanoparticle (R_{PS}) and number of hard disks (N) were fixed at the beginning of the simulation and the scheme allowed for displacement and density moves, in which the half spheres' radius (R_{HS}) was increased until equilibrium was reached. We obtained the optimal number of hard spheres (N_{op}) as the value at which the ratio $|R_{HS}/R_{PS}|$ at equilibrium matched the experimental value. In our case, $N_{op} = 90$. Subsequently, we calculated the molecular weight of a raspberry particle by taking the density of the polyacrylate to be 1.2 g/cm^3 and the density of polystyrene to be 1.05 g/cm^3. We then measured the density of our 3 wt % raspberry nanoparticle stock solution and used this information to determine the concentration to be 3 nmol/L. The molar concentrations of the positively and negatively charged PS nanoparticles were estimated by calculating the molecular weight of the 45 and 280 nm large PS particles using the density of the polymer to be 1.05 g/cm^3. We next measured the density of the 5 wt % nanoparticle solution and estimated the molar concentration to be 500 nM. The concentration of the InP/ZnS quantum dots was estimated using the absorption cross section given in ref 28.

Formation of Solid Films. Prior to film formation, nanoparticles (negatively charged PS particles, positively charged PS nanoparticles, or InP/ZnS quantum dots) were mixed with raspberry particles. The final concentration of raspberry particles was kept constant at 0.3 nM in all mixtures, while the nanoparticle concentrations in the mixtures were 0, 50, 250, 500, or 1250 nM. The total volume of all the mixtures was set to 1 mL. Films of these mixtures were prepared in an environment whose temperature was kept constant at around 20 °C. The films were formed on a glass microscope slide, which was cleaned by rinsing it with isopropanol, acetone, and water, by drop-casting 500 μL of the particle dispersion. The dimensions of the films were ~2.5 cm × 3.6 cm. The films are dried for 10 days to ensure that all the water in the samples evaporates.

Structural Characterizations of the Nanoparticles. High angle annular dark field scanning transmission electron microscopy (HAADF STEM) images were taken using an FEI Tecnai Osiris 200 kV transmission electron microscope. Specimens were prepared by drop-casting from solution on a graphene oxide on a lacey carbon Cu grid by EM Resolutions. Scanning electron microscopy (SEM) images were taken with a Zeiss SIGMA VP field emission scanning electron microscope and an FEI Nova field emission scanning electron microscope. To take the cross-section images, samples were first drop-casted on an aluminum foil, and then, the dry film was cut and Au/Pd was sputtered onto the film prior to imaging using an Emitech K575X sputterer at a current of 50 mA for 15 s. The estimated metal thickness was ~3.8 nm. The thickness and roughness of the samples

https://dx.doi.org/10.1021/acs.langmuir.9b01014
Langmuir 2020, 36, 911−918

were measured using a Bruker DektakXT Benchtop Stylus profilometer. For each sample, the measurement length exceeded 1.5 cm for all the samples.

Optical Characterizations. Absorbance measurements of the QD and transmittance measurements of the films were taken using a Cary 100 UV−vis spectrophotometer. An uncoated microscope slide was used to measure the baseline. At least three transmittance measurements were taken at different locations of the films to average out the effects of the surface morphology differences on the solid films. The reported transmission spectra in the manuscript are the averages of these measurements unless otherwise stated. Reflectance measurements were recorded using an Olympus BX60 microscope equipped with a Thorlabs CCS 100 spectrometer and a halogen light source by using a standard reflection sample as reference. A 20× objective with a 0.75 numerical aperture was employed. Optical microscope images were taken using the same microscope equipped with a Zeiss AxioCam MRc5 camera. At this point, it is worth pointing out that the transmission measurements were taken out using a UV−vis spectrometer collecting almost only a normal signal, whereas the reflection measurements were carried out using the optical microscope equipped collecting the light over a larger angular distribution. Therefore, the sum of reflection and transmission may seem to exceed unity if the difference in two configurations is missed.

RESULTS AND DISCUSSION

Our raspberry particles shown in Figure 1a are composed of a 200 nm sized polystyrene particle surrounded by 45 nm sized

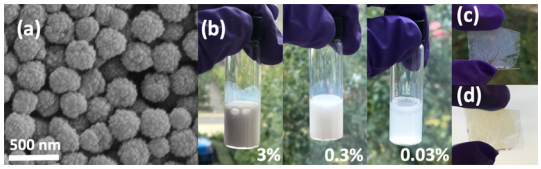

Figure 1. (a) SEM image of RB particles. (b) Photographs of RB particle aqueous dispersions at concentrations of 3, 0.3, and 0.03 wt %. (c, d) Photographs of the RB particle solid film at different angles.

polyacrylate hemispheres. We synthesized them by cross-linking acrylate and styrene using divinylbenzene in a water−ethanol solution.[24] Their large size and high refractive index difference between the RB material ($n_{Polystyrene}$ = 1.6, $n_{Acrylate}$ = 1.49) and water (n_{Water} = 1.33), together with the surface roughness contribute to the strong scattering, giving their dispersions a milky appearance even when they are very dilute (Figure 1b). Interestingly, a red reflection band emerges at certain angles in dry, solid films due to Bragg reflections when the RB particles are densely packed[24] while appearing white at other angles (Figure 1c,d).

To suppress this strong scattering in solid films, we hybridized our positively charged RBs with nanoparticles having various physical characteristics. First, we employed negatively charged 45 nm sized polystyrene (PS) nanoparticles, which are similarly sized as the bumps on the RBs. To study the effect of the added nanoparticle amount, we varied the ratio of the PS particles to RB particles, as shown in Table 1. The final concentration of the raspberry particles in the final solution became 0.3 wt %, which we estimate to correspond to ∼0.3 nM, while the estimated molarity of the small PS particles varied between 50 and 1250 nM. After mixing both types of particles at certain ratios, we left them to interact for 2 h and then drop-cast the suspension onto a microscope slide. The final surface area of the prepared films was ∼9 cm^2.

As shown in Figure 2, the film prepared without negatively charged PS nanoparticles exhibits strong scattering, leading to

Table 1. Number of RB Particles and Negatively Charged PS Particles in all the Mixtures along with the Number of PS Particles per RB Particle and the Ratio of the RB Particle and PS Particles of Different Samples

sample no.	RB particle (pmol)	PS particle (pmol)	number of PS particles per RB particle	ratio of PS to RB particle volume
1	0.3		0	0
2	0.3	50	173	1.26
3	0.3	250	865	6.28
4	0.3	500	1730	12.6
5	0.3	1250	4325	31.4
6		250	N/A	N/A

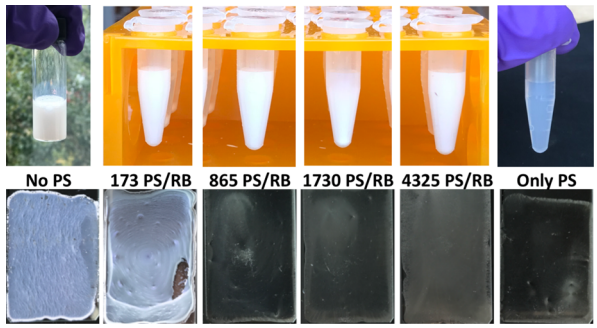

Figure 2. Photographs of pure RB suspensions (left, upper row) and the hybrid samples with varying negatively charged PS-to-RB particle ratios and only negatively charged PS particle dispersions (right, upper row) and the respective drop-cast solid films (lower row).

a white appearance. However, increasing the ratio of PS nanoparticles to RB particles increases the transparency of the films. Our measurements show that the film made of only RB particles has an average transmission above 70% at longer wavelengths, whereas this transmission quickly decreases down to 50% at 550 nm and to 15% at 400 nm (Figure 3). We

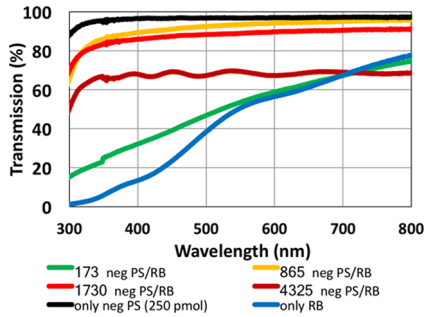

Figure 3. Averaged transmission spectra of the solid films employing RB and negatively charged PS particles (neg PS) at various particle number ratios.

observe that the addition of oppositely charged PS to RB particles first affects the transmission in the blue ultraviolet regime. For example, the sample prepared using a ratio of 173 PS particles per RB particles (1.26 PS-to-RB volume ratio) shows almost 30% transmission at 400 nm, while the transmission at 550 and 800 nm remains almost the same as that in pure RB particle films. A further increase of the negatively charged PS-to-RB ratio to 865 (6.28 PS-to-RB volume ratio) dramatically boosted the transparency of the film to above 90% between 420 and 800 nm. Interestingly, further

https://dx.doi.org/10.1021/acs.langmuir.9b01014
Langmuir 2020, 36, 911−918

increasing the PS-per-RB ratio to 1730 (12.6 PS-to-RB volume ratio) caused a slight decrease in the transmission of the film, while a more profound increase in the PS particle number further pushes down the transmittance levels. That decrease was accompanied by the appearance of a resonant behavior in the transmission spectra. Since the data presented in Figure 3 are averaged over the measurements taken at different parts of the film, the resonant behavior seemed to be averaged out. These resonances can be seen more clearly in individual transmission spectra presented in Figure S1. A clear periodicity is also apparent when the transmission spectra are drawn against the photon energy rather than the wavelength (Figure S1).

To have a better understanding of the observed effects, we turned our attention to the film morphology and first imaged the surface of the films using optical microscopy (Figure 4).

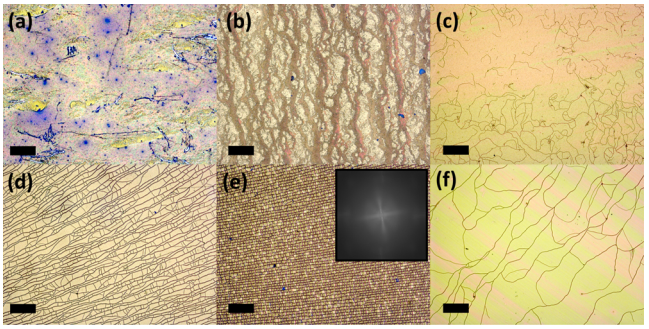

Figure 4. Optical microscopy images of the dried films made of (a) only raspberry particles along with hybrid samples prepared using (b) 173, (c) 865, (d) 1730, and (e) 4325 negatively charged polystyrene particles per raspberry particles with the fast Fourier transform of the image (inset) and (f) dry film of the negatively charged polystyrene particles. Scale bars, 200 μm.

We found that the films composed of only RB particles have rough surfaces with a brown-reddish appearance supporting our previous work.[24] In the sample prepared using a ratio of 865 PS per RB particle (corresponding to 6.28 volume ratio of particles), the surface scatters more weakly compared to the film prepared solely from RB particles and strongly resembles the film made of only PS particles. Further increasing the PS nanoparticle content interestingly causes the occurrence of cracking patterns that do not develop in the films made of only small PS nanoparticles. These cracks become denser and more regular when more polystyrene particles are employed. In the literature, the appearance of cracks in drying colloidal films is well understood and attributed to the capillary pressure buildup in the drying films, as discussed in refs 29 and 30. We observe more resonance peaks accompanied by increased reflection at the locations of the film where these cracks are denser (Figure S2). Thus, the observed resonant behavior in reflection and transmission seems to be related to the occurrence of these regular cracks. Nevertheless, further investigation is definitely needed to reach a final conclusion, which is out of focus of this particular work. On the other hand, optical microscopy shows that films prepared using certain RB-per-PS ratios scatter weakly and appear to have smoother surfaces, while the crack formation at higher PS loadings increases the reflection and decreases the transmission.

To reveal the relation of the observed transparency and the film surface, we turned our attention to the film roughness measured using a profilometer. As presented in Table 2, the

Table 2. Average Thickness and Roughness of the Films Made of Negatively Charged PS Particles and Positively Charged RB Particles[a]

sample no.	number of PS particles per RB Particle	thickness (μm)	roughness (μm)	roughness (%)
1	0	1.17	0.35	30
2	173	8.07	3.35	42
3	865	4.75	1.37	29
4	1730	4.76	2.32	49
5	4325	10.5	9.33	89
6	N/A (only PS)	2.19	0.68	31

[a]The percentage roughness is calculated by taking the ratio of the absolute roughness values to thickness values. These measurements were taken using a Stylus profilometer over a length of at least 1.5 cm. The average thickness was found by measuring the height difference between the coated and uncoated parts of the glass, and the roughness was found by measuring the average deviations around the mean line.

surface roughness of the RB particle film is about 350 nm, which is similar to the size of a single RB particle. We see that, at first, the surface roughness and the film thickness increase upon the addition of oppositely charged PS particles. As we further add negatively charged PS particles to the RBs, we obtain a minimum roughness and roughness-to-thickness ratio, which perfectly matches with the sample having the highest transmission. After this ratio, the roughness again increases to incredibly high values (>9 μm in the 4325 PS-to-RB ratio) accompanied by a decreased transmittance. The recorded roughness can be partially attributed to high thickness values, as also shown by Jeon et al.[31] Another cause of the increased roughness could be the formation of larger particle collections of electrostatically attracted PS and RBs. As the film dries, these larger particle collections could get closer to each other, leading to an even increased roughness. In addition to this, optical microscopy images (Figure 4) indicate denser cracks at high concentrations of PS particles in the hybrid films. These cracks also contribute to increased roughness readings, and we expect them to further strengthen the scattering. Moreover, as shown in the transmission spectra (Figure 3), these samples with dense cracks possess regular transmission peaks, indicating the creation of reflection bands in the film, which should further decrease the transmission.

At this point, our experimental results have an interesting feature: the transmission of the films increases despite the almost 10× increasing surface roughness upon the addition of oppositely charged PS particles to the RB particles. Contrary to our results, we would normally expect the surface roughness to boost the optical scattering, leading to a white appearance. This is mainly because the surface roughness is usually linked to the spatial variation of the refractive index that is the real driving force behind the scattering process in films. In the light of this fact, we believe that, in our films, the scattering weakens and the transparency improves because spatial variation of refractive index inside the film is suppressed. We hypothesize that the electrostatic attraction between oppositely charged colloids enabled the smaller PS particles to move closer to the larger RB particles in dry films and did not allow the formation of big regions of air gaps that would create high refractive index contrast. As a result, the spatial variation of the refractive index

https://dx.doi.org/10.1021/acs.langmuir.9b01014
Langmuir 2020, 36, 911−918

remained smaller inside the film, leading to an improved transparency in spite of a significant film roughness, which still should contribute to scattering. Nevertheless, as the number of negatively charged PS particles per RB increases, the surface roughness further increases and denser regular cracks appear. The increasing surface roughness (which also includes the cracks) strengthens the scattering. On top of this, the regular cracks create reflection bands (as indicated by the periodic features in the transmission curve of the 4325 PS-to-RB sample). We believe that all these effects together decrease the film transmissions in the samples having more than the 865 PS-to-RB ratio.

To gain further information on the film morphology and its relation to increased transparency, we took the SEM images of our hybrid films. SEM images of the surface of the only RB film shows that these particles ended up very close to each other while also possessing regions void of any particles when the film dried (Figure 5). On the other hand, in the hybrid film

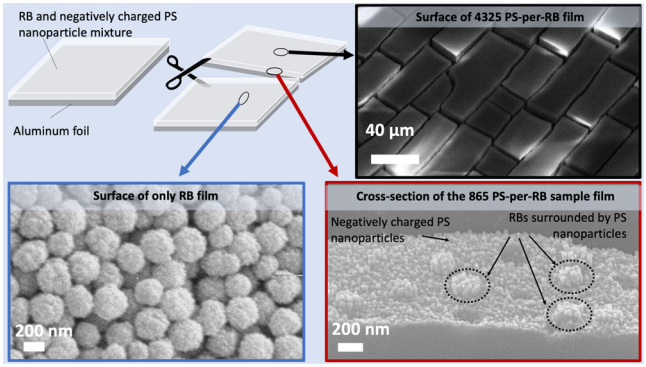

Figure 5. Scanning electron microscopy images of hybrid films. Illustration of the sample preparation (top left), surface SEM image of the only RB film (bottom left), cross-sectional SEM image of the RB and negatively charged PS nanoparticle film prepared using the 865 PS-to-RB particle ratio (bottom, right), and SEM image of the hybrid film surface (4325 PS-to-RB particle ratio; top, right).

made of the 865 PS-per-RB sample (6.28 PS-to-RB volume ratio), we do not observe these void regions; on the contrary, we see that the smaller PS particles surround the RB particles, which are attracted to each other due to electrostatic interaction. In addition to the absence of the voids within the film, these smaller PS nanoparticles seem to have avoided the aggregation of RBs. Both of these effects also appear to have a strong role in the suppressed scattering of raspberries.

To reveal whether the negatively charged PS particles surrounding the RBs or the PS nanoparticles forming a sea of small weakly scattering particles is dominant in the observed effect, we carried out a control experiment. For this purpose, we mixed negatively charged PS particles and RBs such that the PS-to-RB particle number ratio is 1250. After 2 h, we centrifuged the mixture at a low speed (1000 rpm), removed the supernatant containing the small PS particles, and then redispersed the precipitate containing RB particles surrounded by PS particles in deionized water. After repeating this procedure five times, we prepared a film of the PS-coated RB particle solution by drop-casting onto a glass substrate. As presented in Figure S3, the transparency of the film has slightly improved compared to the only RB film but still remained much worse compared to the case without centrifugation. This result showed that, while the PS particles sitting on the RB particle surface seem to have a role on the observed improvement in transparency, a significant contribution comes from the smaller nanoparticles forming a transparent medium, including RB particles that have very limited optical interaction with each other.

To test the effect of the nanoparticle charge on the optical properties of the films, we mixed our positively charged RB particles with positively charged 45 nm PS particles. As opposed to the films with oppositely charged PS particles, these films did not become transparent, as shown in Figure S4. Their transmission spectra (Figure S5) did not show any profound improvement; nevertheless, the reflection spectra measured with an optical microscope revealed an increased reflectance with an increasing positively charged PS particle content (Figure S6). The optical microscopy images shown in Figure S7 indicate the formation of the film with irregular dense cracks when a small number of PS particles are employed. Increasing the ratio of PS particles to raspberry particles triggered the formation of regular crack patterns on the film surface accompanied by increased reflection and a resonant behavior, similar to the films where negatively charged PS particles were employed. As shown in the SEM images (Figure S7), the cracks developed in this hybrid system and contributed to decreased transparency. Different than the case with negatively charged PS particles, we were unable to clearly reckon single RBs in the films made of positively charged PS particles hybridized with RBs (Figure S8). Furthermore, the cross section of the film seems to be significantly rough and irregular, unlike the case of negatively charged particles. This indicates that there are differences in the drying process and very likely in distribution of particles, although we could not clearly identify aggregates of RBs. We have also studied the roughness of these films using a profilometer. The results presented in Table 3 show that the

Table 3. Average Thickness and Roughness of the Hybrid Films of Positively Charged PS Particles and Positively Charged RB Particles[a]

number of PS particles per RB particle	thickness (μm)	roughness (μm)	roughness (%)
0	1.17	0.35	30
173	2.47	0.85	35
865	3.07	1.03	35
1730	5.00	1.05	21
N/A (only PS)	2.34	0.63	30

[a]The percentage roughness is calculated by taking the ratio of the absolute roughness values to thickness values. These measurements were taken using a Stylus profilometer over a length of at least 1.5 cm. The average thickness was found by measuring the height difference between the coated and uncoated parts of the glass, and the roughness was found by measuring the average deviations around the mean line.

hybrid films made of positively charged PS and RBs have similar thickness and roughness features as their counterparts prepared using negatively charged PS particles. We, therefore, believe that the observed difference in transparency stems from how positively and negatively charged PS particles are distributed in the presence of positively charged RBs. We hypothesize that the presence of electrostatic repulsion in the positively charged PS−RB hybrids does not enable the formation of a relatively smooth spatial refractive index profile inside the film and create large void regions; thus, these films remain significantly scattering while their counterparts are

https://dx.doi.org/10.1021/acs.langmuir.9b01014
Langmuir 2020, 36, 911−918

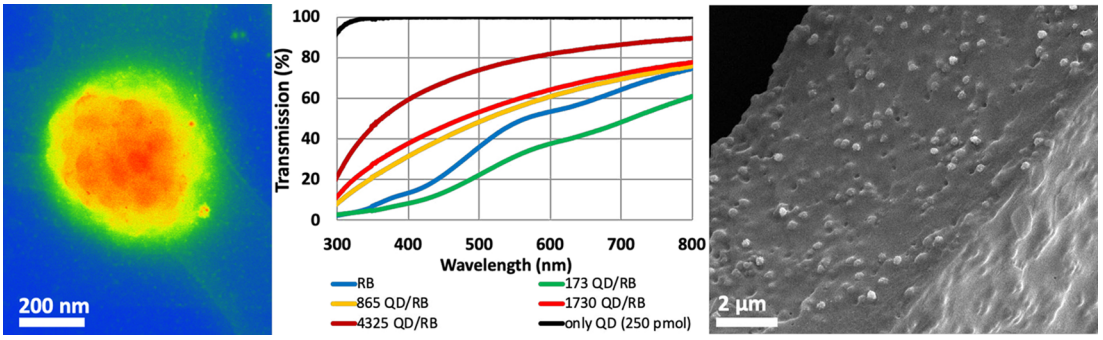

Figure 6. (Left) Colored HAADF STEM image of RB and quantum dot (QD) hybrid (4325 quantum dots per RB particle sample). (Middle) Transmission spectra of the films made of quantum dot and RB particles hybridized at different number ratios. (Right) SEM image of the RB particle and quantum dot hybrid (4325 quantum dots per RB particle sample).

transparent despite the similarities in film thickness and surface roughness.

Here, we also hybridized our positively charged RBs with oppositely charged semiconductor InP/ZnS core/shell quantum dots. These materials have a size of ∼10 nm constituting of an InP core with a refractive index of 3.5−4.4 and a shell material of ZnS with a refractive index of 2.3−2.5 in the visible regime. As a result, the effective refractive index of these quantum dots should be significantly higher than that of the PS particles, which is around 1.6. Nevertheless, the polymer coating used during the phase transfer should make the effective refractive index of these particles close to the refractive index of RB particles. Thus, we would expect increased overall optical transmittance in these hybrid films of RBs and quantum dots.

The dark field scanning transmission electron microscopy images presented in Figure 6a and Figure S9 indicate that the carboxyl-functionalized quantum dots successfully surround the surface of the raspberry particles, similar to the films prepared using negatively charged PS particles. Additionally, the polymer stabilizing the quantum dots enveloped the raspberries to the point that the optical features of these films started to resemble those made of the negatively charged PS particles (compare spectra in Figures 3 and 6). However, different to the films with PS particles, we observed a slight decrease in the average transmission of the film prepared using a ratio of 173 quantum dots per RB particle compared with the film prepared from only RB particles alone. Further addition of quantum dots triggered a strong increase in the transparency of the films, especially in the long wavelength regime, while the absorption of the quantum dots does not allow the transmission to increase significantly in the short wavelength regime. In contrast to negatively charged PS−RB particle hybrids, here, we did not see any resonant behavior in the transmission spectra. The optical microscopy images reveal that the surface roughness of the hybrid films remains high when the amount of quantum dots is low (Figure S10), which explains the low transmission. Further increasing the amount of quantum dots per RB particle avoids the aggregations of raspberry particles as the smaller quantum dots surround the oppositely charged RBs (Figure 6). Similar to the hybrid films prepared with PS particles, these films also exhibited a high transmittance despite the rough surface. We think that the quantum dots that are coated with polymer enabling their dispersions in aqueous solutions may have contributed to a much smoother refractive index variation in nanometer and micrometer scales. Furthermore, these quantum dot-RB hybrid films do not have big regions void of particles similar to the hybrids of PS−RB particles and the RB particles that are clearly surrounded by the oppositely charged quantum dots. Another interesting observation is the lack of the crack formation. This explains the absence of resonant behavior and also contributes to the improved transmittance in addition to the absence of void regions and quantum dots surrounding the RBs such that RBs do not form aggregates. Although it is not the focus of this work, it is here worth mentioning that these thin films with QDs exhibited photoluminescence detectable by eye when excited with a UV lamp. On the other hand, their absorption features were not very obvious from the transmission spectra, which we attribute to the low thickness of our films as well as to the limitations of our measurement system.

To understand whether the large surface area and the roughness of the raspberry particles play a role on the observed optical properties, we carried out a control experiment employing 280 nm sized, positively charged, smooth polystyrene spheres instead of RBs. We hybridized these large particles with 45 nm sized oppositely charged polystyrene particles and formed their films. The photos and optical microscope images of the films presented in Figures S11 and S12 show that smaller negatively charged PS particles have a profound effect on the transmission of the films with these large polystyrene particles, as was the case with RBs. Furthermore, the transmission measurements reveal that, upon addition of the small nanoparticles, the transmission in short wavelengths increased significantly, which is similar to RB and negatively charged PS particle hybrid films (Figure S13). Finally, the transmission levels and the trends of the transmission were similar to the films made of RB particles alone. On the other hand, the surface roughness of the hybrid films made of larger and smaller PS particles is around 0.45 μm (for the 865 small-to-large particle number ratio), corresponding to 45%. These results show that the smaller particles surrounding the larger particle owing to electrostatic attraction still improve the transmittance despite the high surface roughness, again indicating low refractive index variation in the film. Similar to the sample prepared with RB negatively charged PS samples, we observed cracks also in these hybrid films of large positively charged PS and small negatively charged PS films. When one of the particles in the hybrid (large or small ones) was absent, these cracks did not form. The cracks did not form in the case that the quantum dots were employed instead of negatively charged PS particles. This brings us to the conclusion that the presence of smaller PS

https://dx.doi.org/10.1021/acs.langmuir.9b01014
Langmuir 2020, 36, 911−918

particles regardless of their charge together with a larger particle triggers the formation of the cracks.

CONCLUSIONS

In this work, we developed a simple strategy to obtain transparent films of highly scattering particles. With this motivation, we studied raspberry particles as a good example of strongly scattering nanoparticles. We found that solid films prepared from these scattering particles can be made transparent upon hybridization with oppositely charged smaller nanoparticles, which can also form transparent films alone. Our experiments revealed that oppositely charged smaller nanoparticles surround the surface of the larger, strongly scattering particles on account of electrostatic interactions and avoid aggregation of large particles during the drying process. This leads to a smoother spatial refractive index profile by avoiding the formation of void regions inside the film. Despite the large surface roughness, this aids the transmittance of the films to increase. Our experiments with smaller nanoparticles having the same charge as the scattering particles indicated that it was critical to use oppositely charged particle systems to induce transparency as aggregation could be avoided. Finally, we revealed that the observed transparency upon hybridization does not depend on the shape of the large particles based on our experiments with large spherical and raspberry particles. We believe that the simple methodology for enabling transparency explored here may prove useful for various types of scattering organic and inorganic nanoparticles in optical coatings or optoelectronic devices in the future.

ASSOCIATED CONTENT

Supporting Information

The Supporting Information is available free of charge at https://pubs.acs.org/doi/10.1021/acs.langmuir.9b01014.

Transmission spectra of the solid films of RBs and negatively charged PS as a function of wavelength and photon energy, averaged reflection spectra of the films with RB and negatively charged PS, photograph of the solid films, transmission and reflection spectra of the solid films of positively charged PS particles and RB particle hybrids, optical microscopy images of the solid films of positively charged PS particles and RB particle hybrids, SEM images of the films of positively charged PS particles and RB hybrid films, absorption and photoluminescence spectra of the quantum dots, TEM image of RBs surrounded by quantum dots, optical microscopy images and photographs of the solid films of the RB quantum dot hybrid samples, optical microscopy images, and transmission spectra of the RB large PS hybrid films (PDF)

AUTHOR INFORMATION

Corresponding Authors

Talha Erdem − *Cavendish Laboratory, Department of Physics, University of Cambridge, Cambridge CB3 0HE, United Kingdom;* orcid.org/0000-0003-3905-376X; Email: te294@cam.ac.uk

Erika Eiser − *Cavendish Laboratory, Department of Physics, University of Cambridge, Cambridge CB3 0HE, United Kingdom;* orcid.org/0000-0003-2881-8157; Email: ee247@cam.ac.uk

Authors

Lan Yang − *Melville Laboratory for Polymer Synthesis, Department of Chemistry, University of Cambridge, Cambridge CB2 1EW, United Kingdom*

Peicheng Xu − *Cavendish Laboratory, Department of Physics, University of Cambridge, Cambridge CB3 0HE, United Kingdom*

Yemliha Altintas − *Departments of Electrical-Electronics Engineering and Materials Science and Nanotechnology Engineering, Abdullah Gül University, Kayseri 38080, Turkey*

Thomas O'Neil − *Cavendish Laboratory, Department of Physics, University of Cambridge, Cambridge CB3 0HE, United Kingdom*

Alessio Caciagli − *Cavendish Laboratory, Department of Physics, University of Cambridge, Cambridge CB3 0HE, United Kingdom*

Caterina Ducati − *Department of Material Science and Metallurgy, University of Cambridge, Cambridge CB3 0FS, United Kingdom;* orcid.org/0000-0003-3366-6442

Evren Mutlugun − *Departments of Electrical-Electronics Engineering and Materials Science and Nanotechnology Engineering, Abdullah Gül University, Kayseri 38080, Turkey;* orcid.org/0000-0003-3715-5594

Oren A. Scherman − *Melville Laboratory for Polymer Synthesis, Department of Chemistry, University of Cambridge, Cambridge CB2 1EW, United Kingdom;* orcid.org/0000-0001-8032-7166

Complete contact information is available at: https://pubs.acs.org/10.1021/acs.langmuir.9b01014

Funding

Royal Society Newton International Fellowship.

Notes

The authors declare no competing financial interest.

ACKNOWLEDGMENTS

T.E. acknowledges the Royal Society for the Newton International Fellowship. We also thank Peian Li for optimizing the polystyrene nanoparticle syntheses.

REFERENCES

(1) Gaponenko, S. V.; Demir, H. V. *Applied Nanophotonics;* Cambridge University Press: Cambridge, 2018.

(2) Zhao, Y.; Wang, J.; Mao, G. Colloidal subwavelength nanostructures for antireflection optical coatings. *Opt. Lett.* **2005**, *30*, 1885−1887.

(3) Erdem, T.; Demir, H. V. Colloidal nanocrystals for quality lighting and displays: milestones and recent developments. *NANO* **2016**, *5*, 74−95.

(4) Erdem, T.; Demir, H. V. Color science of nanocrystal quantum dots for lighting and displays. *NANO* **2013**, *2*, 57−81.

(5) Kim, Y.; Johnson, R. C.; Hupp, J. T. Gold Nanoparticle-Based Sensing of "Spectroscopically Silent" Heavy Metal Ions. *Nano Lett.* **2001**, *1*, 165−167.

(6) Lal, S.; Link, S.; Halas, N. J. Nano-optics from sensing to waveguiding. *Nat. Photonics* **2007**, *1*, 641−648.

(7) Tuncel, D.; Demir, H. V. Conjugated polymer nanoparticles. *Nanoscale* **2010**, *2*, 484−494.

(8) Wu, C.; Bull, B.; Christensen, K.; McNeill, J. Ratiometric single-nanoparticle oxygen sensors for biological imaging. *Angew. Chem., Int. Ed.* **2009**, *48*, 2741−2745.

(9) Atwater, H. A.; Polman, A. Erratum: Plasmonics for improved photovoltaic devices. *Nat. Mater.* **2010**, *9*, 865−865.

(10) Ning, Z.; Ren, Y.; Hoogland, S.; Voznyy, O.; Levina, L.; Stadler, P.; Lan, X.; Zhitomirsky, D.; Sargent, E. H. All-Inorganic Colloidal Quantum Dot Photovoltaics Employing Solution-Phase Halide Passivation. *Adv. Mater.* **2012**, *24*, 6295−6299.
(11) Sargent, E. H. Colloidal quantum dot solar cells. *Nat. Photonics* **2012**, *6*, 133−135.
(12) Hu, W.; Bai, F.; Gong, X.; Zhan, X.; Fu, H.; Bjornholm, T. *Organic optoelectronics*; Wiley-VCH Verlag GmbH & Co. KGaA: Berlin, 2013.
(13) Coe-Sullivan, S. Quantum dot developments. *Nat. Photonics* **2009**, *3*, 315−316.
(14) Henglein, A. Electronics of Colloidal Nanometer Particles. *Berich. Bunsen. Gesell.* **1995**, *99*, 903−913.
(15) Rahim, N. A. A.; McDaniel, W.; Bardon, K.; Srinivasan, S.; Vickerman, V.; So, P. T. C.; Moon, J. H. Conjugated Polymer Nanoparticles for Two-Photon Imaging of Endothelial Cells in a Tissue Model. *Adv. Mater.* **2009**, *21*, 3492−3496.
(16) Bera, D.; Qian, L.; Tseng, T.-K.; Holloway, P. H. Quantum Dots and Their Multimodal Applications: A Review. *Materials* **2010**, *3*, 2260−2345.
(17) Feng, L.; Zhu, C.; Yuan, H.; Liu, L.; Lv, F.; Wang, S. Conjugated polymernanoparticles: preparation, properties, functionalization and biological applications. *Chem. Soc. Rev.* **2013**, *42*, 6620−6633.
(18) Huang, G.; Li, H.; Chen, J.; Zhao, Z.; Yang, L.; Chi, X.; Chen, Z.; Wang, X.; Gao, J. Tunable T1 and T2 contrast abilities of manganese-engineered iron oxide nanoparticles through size control. *Nanoscale* **2014**, *6*, 10404−10412.
(19) Jamieson, T.; Bakhshi, R.; Petrova, D.; Pocock, R.; Imani, M.; Seifalian, A. M. Biological applications of quantum dots. *Biomaterials* **2007**, *28*, 4717−4732.
(20) Gandra, N.; Portz, C.; Nergiz, S. Z.; Fales, A.; Vo-Dinh, T.; Singamaneni, S. Inherently Stealthy and Highly Tumor-Selective Gold Nanoraspberries for Photothermal Cancer Therapy. *Sci. Rep.* **2015**, *5*, 10311.
(21) Ragosta, G.; Abbate, M.; Musto, P.; Scarinzi, G.; Mascia, L. Epoxy-silica particulate nanocomposites: Chemical interactions, reinforcement and fracture toughness. *Polymer* **2005**, *46*, 10506−10516.
(22) Song, Y.; Bi, C.; Wu, C.; He, H.; Huang, L.; Wang, D.; Xia, H. Promoting charge transfer in hyperbranched, trisoctahedral-shaped core-shell Au@PdPt nanoparticles by facet-dependent construction of transition layers as high performance electrocatalysts. *J. Mater. Chem. A* **2017**, *5*, 18878−18887.
(23) Li, C.; Kattawar, G. W.; Yang, P. Effects of surface roughness on light scattering by small particles. *J. Quant. Spectrosc. Radiat. Transfer* **2004**, *89*, 123−131.
(24) Lan, Y.; Caciagli, A.; Guidetti, G.; Yu, Z.; Liu, J.; Johansen, V. E.; Kamp, M.; Abell, C.; Vignolini, S.; Scherman, O. A.; Eiser, E. Unexpected stability of aqueous dispersions of raspberry-like colloids. *Nat. Commun.* **2018**, *9*, 3614.
(25) Altïntas, Y.; Talpur, M. Y.; Mutlugün, E. Efficient Förster Resonance Energy Transfer Donors of In(Zn)P/ZnS Quantum Dots. *J. Phys. Chem. C* **2017**, *121*, 3034−3043.
(26) Lin, C.-A. J.; Sperling, R. A.; Li, J. K.; Yang, T.-Y.; Li, P.-Y.; Zanella, M.; Chang, W. H.; Parak, W. J. Design of an Amphiphilic Polymer for Nanoparticle Coating and Functionalization. *Small* **2008**, *4*, 334−341.
(27) Tobochnik, J.; Chapin, P. M. Monte Carlo simulation of hard spheres near random closest packing using spherical boundary conditions. *J. Chem. Phys.* **1988**, *88*, 5824−5830.
(28) Shirazi, R. InP/ZnS nanocrystals for colour conversion in white light emitting diodes. PhD. Dissertation, Technical University of Denmark (DTU), May 2013.
(29) Winnik, M. A.; Feng, J. Latex Blends: An Approach to Zero VOC Coatings. *J. Coat. Technol.* **1996**, *68*, 39−50.
(30) Routh, A. F. Drying of thin colloidal films. *Rep. Prog. Phys.* **2013**, *76*, No. 046603.
(31) Jeon, J.; Panchagnula, V.; Pan, J.; Dobrynin, A. V. Molecular Dynamics Simulations of Multilayer Films of Polyelectrolytes and Nanoparticles. *Langmuir* **2006**, *22*, 4629−4637.

https://dx.doi.org/10.1021/acs.langmuir.9b01014
Langmuir 2020, 36, 911−918